Available online at www.sciencedirect.com
SCIENCE DIRECT®
Computer Coupling of Phase Diagrams and Thermochemistry 28 (2004) 354–362
www.elsevier.com/locate/calphad

Thermodynamic evaluation of the phase equilibria and glass-forming ability of the Fe–Si–B system☆

Tatsuya Tokunaga[a,*], Hiroshi Ohtani[b,c], Mitsuhiro Hasebe[b,c]

[a] *Fukuoka Industrial Technology Center, 3-6-1 Norimatsu, Yahatanishi-ku, Kitakyushu 807-0831, Japan*
[b] *Department of Materials Science and Engineering, Kyushu Institute of Technology, 1-1 Sensui-cho, Tobata-ku, Kitakyushu 804-8550, Japan*
[c] *CREST-Japan Science and Technology Agency, Japan*

Received 21 August 2004; received in revised form 15 November 2004; accepted 16 November 2004
Available online 18 December 2004

Abstract

A thermodynamic study has been carried out on the Fe–Si–B ternary system, which is important in the development of transformer core materials and Ni-based filler metals. A regular solution approximation based on the sublattice model was adopted to describe the Gibbs energy for the individual phases in the binary and ternary systems. Thermodynamic parameters for each phase were evaluated by combining the experimental results from differential scanning calorimetry with literature data. The evaluated parameters enabled us to obtain reproducible calculations of the isothermal and vertical section diagrams. Furthermore, the glass-forming ability of this ternary alloy was evaluated by introducing thermodynamic quantities obtained from the phase diagram calculations into Davies–Uhlmann kinetic formulations. In this evaluation, the time–temperature-transformation (TTT) curves were obtained, which are a measure of the time required to transform to the minimum detectable mass of crystal as a function of temperature. The critical cooling rates calculated on the basis of the TTT curves enabled us to evaluate the glass-forming ability of this ternary alloy. The results show good agreement with the experimental data in the compositional amorphization range.

Keywords: CALPHAD; Iron–silicon–boron; Phase equilibria; Glass-forming ability; Amorphous

1. Introduction

Fe–Si–B ternary alloys are important in the development of transformer core materials, Ni-based brazing filler metals, and Ni-based self-fluxing alloys. In particular, information on the phase equilibria involving the liquid phase is necessary, since the glass-forming ability of this alloy is relevant to the liquidus temperatures, and the liquidus and solidus temperatures are important in brazing filler metal applications. Currently, there are no details on the phase equilibria involving the liquid phase.

Amorphous Fe–Si–B alloys are used as transformer core materials due to their good magnetic properties, and the glass-forming ability of these alloys has been studied experimentally [1–4]. The glass-forming ability of these alloys has been evaluated using the time–temperature-transformation (TTT) curves employing the Davies–Uhlmann kinetic formulations [5]. However, the thermodynamic quantities required for input into the Davies–Uhlmann kinetic equations cannot be evaluated precisely. Saunders and Miodownik [6] have evaluated the glass-forming ability of some binary and ternary alloy systems, where the thermodynamic quantities were derived using the constituent binary thermodynamic phase diagram calculations, which were then input into the Davies–Uhlmann kinetic equations. Saunders and Miodownik found reasonable agreement

☆ Presented at CALPHAD XXXIII, Kraków, Poland, May 30–June 4, 2004.

* Corresponding address: Core Research for Evolutional Science and Technology (CREST), Japan Science and Technology Agency, 1-1 Sensui-cho, Tobata-ku, Kitakyushu 804-8550, Japan. Tel.: +81 93 884 3381; fax: +81 93 884 3351.
E-mail addresses: ttokunag@fitc.pref.fukuoka.jp, ttokunag@matsc.kyutech.ac.jp (T. Tokunaga), ohtani@matsc.kyutech.ac.jp (H. Ohtani), hasebe@matsc.kyutech.ac.jp (M. Hasebe).

0364-5916/$ - see front matter © 2004 Elsevier Ltd. All rights reserved.
doi:10.1016/j.calphad.2004.11.004

between the calculated and the experimental glass-forming abilities. Thus, in order to predict the glass-forming ability of alloys, construction of the thermodynamic parameters required to calculate the phase diagrams is useful.

For the phase stability of an amorphous phase, amorphous phases are typically treated as considerably supercooled liquid phases, and several attempts to model an amorphous phase were carried out previously. Saunders evaluated the difference in enthalpy between the liquid and amorphous phases in some metallic systems, and showed that the amorphous phase could be more stable than a supercooled liquid phase [7]. Zhou et al. calculated the thermodynamic functions of liquid and supercooled liquid Cu–Ni–Zr and Al–Cu–Ni–Zr alloys using the association model [8], and Tolochko and Ågren modeled the Gibbs energy for the supercooled Fe–B liquid phase with their own experimental results obtained from DSC measurements [9]. Shao [10] and Liu et al. [11] modeled the stabilization of the amorphous phases with respect to the high temperature liquid phase, where the glass transition was treated as a second-order transformation. In addition, Palumbo et al. carried out the thermodynamic assessment of the Fe–B system in order to describe the glass-forming ability of this system, considering the formation of amorphous and metastable Fe_3B phases [12].

We have examined the phase equilibria in the Fe–Si–B system using both the experimental and the CALculation of PHase Diagrams (CALPHAD) approach [13]. Furthermore, the glass-forming ability of Fe–Si–B alloys has been evaluated by combining the thermodynamic quantities obtained from the phase diagram calculations with the kinetic approach.

2. Experimental

The phase boundaries of the ternary Fe–Si–B system were determined using differential scanning calorimetry (DSC). The starting materials used were Fe (99.998%), Si (99.9%), and B (99%) powders. The alloys were prepared by arc melting cold-pressed pellets in an argon atmosphere. A titanium button was melted to getter any residual oxygen in the chamber before melting the actual charges. The arc-melted alloys were re-melted under vacuum using an induction heater to ensure sample homogeneity. The as-cast alloys were then encapsulated in quartz tubes under vacuum, and then annealed at 900 °C for 18 d before being quenched in water. No chemical analysis on the alloys was conducted, as the weight loss in the preparation of the alloys was generally <1%. The alloy compositions prepared are shown in Table 1. Thermal analysis was carried out using a Seiko EXSTAR6300 DSC (Seiko Instruments Inc., Chiba, Japan) on cylindrical samples heated and cooled in Al_2O_3 crucibles at 5 °C/min under flowing purified argon using an α-Al_2O_3 reference standard. The peak temperature values during heating were adopted in our thermodynamic analysis to avoid any experimental errors caused by supercooling. The peak temperatures obtained during heating are shown in Table 1. In addition to using the DSC data, identification of the phases was performed using X-ray diffraction (XRD) analysis for several quenched alloys.

Table 1
Experimental results on the phase boundaries of Fe–Si–B ternary alloys determined by DSC on heating

Alloy composition (mol%)			Peak temperature (°C)			
Fe	Si	B				
80	10	10	1162			
70	20	10	1117	1121	1141	
65	25	10	1101	1112	1146	
60	30	10	1099	1164	1171	
52	38	10	1176			
70	10	20	1129	1266		
65	10	25	1115	1119	1211	1309
60	10	30	1120	1223	1380	
52	10	38	1162			
65	30	5	1153	1120	1127	1159
65	20	15	1102	1111	1200	
65	15	20	1115	1120	1231	
65	5	30	1119	1125	1273	1359

3. Thermodynamic modeling

There are three ternary compounds in the Fe–Si–B ternary system: Fe_5Si_2B [4,14,15], $Fe_{4.7}SiB_2$ [4,14,15], and $(Fe, Si)_3B$ [14,15]. These compounds were treated as being stoichiometric phases in this study, due to the negligible homogeneity ranges. In view of the negligible solid solubility of the third element [4,14,15], all the binary intermetallic compounds were treated as being pure binary phases. Furthermore, the solid solubility of Fe in the Si diamond phase was not taken into account, due to the negligible solid solubility.

The Gibbs energies of the ternary liquid and fcc phases were described by the conventional regular solution model as follows:

$$\begin{aligned} G_{\mathrm{m}}^{\phi} = {} & x_{\mathrm{B}}\,{}^{0}G_{\mathrm{B}}^{\phi} + x_{\mathrm{Fe}}\,{}^{0}G_{\mathrm{Fe}}^{\phi} + x_{\mathrm{Si}}\,{}^{0}G_{\mathrm{Si}}^{\phi} \\ & + RT(x_{\mathrm{B}}\ln x_{\mathrm{B}} + x_{\mathrm{Fe}}\ln x_{\mathrm{Fe}} + x_{\mathrm{Si}}\ln x_{\mathrm{Si}}) \\ & + x_{\mathrm{B}}x_{\mathrm{Fe}}L_{\mathrm{B,Fe}}^{\phi} + x_{\mathrm{Fe}}x_{\mathrm{Si}}L_{\mathrm{Fe,Si}}^{\phi} \\ & + x_{\mathrm{B}}x_{\mathrm{Si}}L_{\mathrm{B,Si}}^{\phi} + x_{\mathrm{B}}x_{\mathrm{Fe}}x_{\mathrm{Si}}L_{\mathrm{B,Fe,Si}}^{\phi}. \end{aligned} \quad (1)$$

where ${}^{0}G_{i}^{\phi}$ is the lattice stability, and denotes the Gibbs energy of element i in the ϕ phase. The descriptions of the lattice stability parameters were taken from the Scientific Group Thermodata Europe (SGTE) data file [16]. R is the universal gas constant, and x_{B}, x_{Fe}, and x_{Si} are the mole fractions of B, Fe, and Si, respectively. The interaction parameters of the binary systems and ternary system are denoted as $L_{i,j}^{\phi}$ and $L_{\mathrm{B,Fe,Si}}^{\phi}$, respectively.

As regards the bcc phase in the Fe–Si system, Lacaze and Sundman [17] took only B2 ordering into account, and neglected $D0_3$ ordering in their thermodynamic assessment. According to Lacaze and Sundman, the Gibbs energy of the bcc phase can be represented using the two-sublattice model [18] with the formula $(Fe, Si)_{0.5}(Fe, Si)_{0.5}$. The Gibbs energy of the bcc phase is described by the following equation [19]:

$$G_m^{bcc} = G_m^{dis\_bcc} + \Delta G_m^{ord\_bcc}(y_i^s) \tag{2}$$

where $G_m^{dis\_bcc}$ is the Gibbs energy of the disordered state, and is described using the regular solution approximation, similar to Eq. (1). The term $\Delta G_m^{ord\_bcc}(y_i^s)$ is the ordering energy, which is zero when the phase is disordered. The ordering energy is given by the following equation:

$$\Delta G_m^{ord\_bcc}(y_i^s) = G_m^{ord\_bcc}(y_i^s) - G_m^{ord\_bcc}(y_i^s = x_i) \tag{3}$$

where $G_m^{ord\_bcc}(y_i^s)$ is the Gibbs energy described using the compound energy formalism given by the following equation:

$$\begin{aligned} G_m^{ord\_bcc}(y_i^s) = {} & y_{Fe}^1 y_{Fe}^2 \,{}^{\circ}G_{Fe:Fe}^{ord\_bcc} + y_{Fe}^1 y_{Si}^2 \,{}^{\circ}G_{Fe:Si}^{ord\_bcc} \\ & + y_{Si}^1 y_{Fe}^2 \,{}^{\circ}G_{Si:Fe}^{ord\_bcc} + y_{Si}^1 y_{Si}^2 \,{}^{\circ}G_{Si:Si}^{ord\_bcc} \\ & + 0.5RT(y_{Fe}^1 \ln y_{Fe}^1 + y_{Si}^1 \ln y_{Si}^1) \\ & + 0.5RT(y_{Fe}^2 \ln y_{Fe}^2 + y_{Si}^2 \ln y_{Si}^2) \\ & + {}^{ex}G^{bcc} \end{aligned} \tag{4}$$

where y_i^s denotes the site fraction of element i on the sth sublattice. ${}^{\circ}G_{i:j}$ denotes the Gibbs energy of a hypothetical compound ij. ${}^{ex}G^{bcc}$ is the excess Gibbs energy term containing the energy of interaction between unlike atoms, and is expressed by the following equation:

$$\begin{aligned} {}^{ex}G^{bcc} = {} & y_{Fe}^1 y_{Si}^1 y_{Fe}^2 L_{Fe,Si:Fe} + y_{Fe}^1 y_{Si}^1 y_{Si}^2 L_{Fe,Si:Si} \\ & + y_{Fe}^2 y_{Si}^2 y_{Fe}^1 L_{Fe:Fe,Si} + y_{Fe}^2 y_{Si}^2 y_{Si}^1 L_{Si:Fe,Si} \end{aligned} \tag{5}$$

where $L_{i,j:k}$ (or $L_{i:j,k}$) is the parameter for interaction between unlike atoms on the same sublattice. $G_m^{ord\_bcc}(y_i^s = x_i)$ is the order-independent contribution of $G_m^{ord\_bcc}(y_i^s)$. In this study, the Gibbs energy of the bcc phase in the Fe–Si–B ternary system was described using two sublattices, denoted by the formula $(Fe, Si, B)_{0.5}(Fe, Si, B)_{0.5}$, after Eq. (2).

The Gibbs energies of the ternary compound phases, $Fe_aSi_bB_c$, were described as follows:

$$\begin{aligned} G_m^{Fe_aSi_bB_c} = {} & a \cdot {}^0G_{Fe}^{bcc} + b \cdot {}^0G_{Si}^{diamond} \\ & + c \cdot {}^0G_B^{\beta\_rhombohedral} + \Delta G_{Fe_aSi_bB_c}^f. \end{aligned} \tag{6}$$

where $\Delta G_{Fe_aSi_bB_c}^f$ is the Gibbs energy of formation per mole of formula unit of the compound, and is expressed by the following equation:

$$\Delta G_{Fe_aSi_bB_c}^f = A + B \cdot T. \tag{7}$$

4. Kinetic formulations

The critical cooling rate for the glass formation can be determined accurately through the construction of a continuous-cooling-transformation (CCT) curve rather than the TTT curve. For instance, the critical cooling rate for the $Pd_{40}Cu_{30}Ni_{10}P_{20}$ alloy would be overestimated to be a factor of 10 by using the TTT curve [20]. However, following many papers, e.g. [6], we evaluated the critical cooling rate through the construction of the TTT curve using the Davies–Uhlmann formulations [5], for steady state homogeneous nucleation. As regards the nucleation in a supercooled liquid, although the importance of transient effects in glass formation was reported by Kelton and Greer [21] and Shao and Tsakiropoulos [22], the effect of the transient state was neglected in this study.

In the Davies–Uhlmann treatment, the time, t, required for the formation of a crystalline phase of volume fraction X is given by following equation:

$$t \approx \frac{9.3\eta}{kT} \left\{ \frac{a_0^9 X}{f^3 N_v} \frac{\exp(G^*/kT)}{[1 - \exp(-G_m/RT)]^3} \right\}^{1/4} \tag{8}$$

where η is the viscosity of the melt, k is Boltzmann's constant, T is the transformation temperature, a_0 is the atomic diameter, N_v is the number of atoms per unit volume, and R is the universal gas constant. The fraction of sites on the interface where atoms may preferentially be added and moved is denoted by f, and is given by the following expression [23]:

$$f \approx 0.2(T_m - T)/T_m \tag{9}$$

where T_m is the liquidus temperature. G_m is the molar free energy driving force for liquid to crystal growth. G^* is the free energy barrier for nucleation of a spherical nucleus, and is given by the expression

$$G^* = \frac{16\pi}{3N}(\sigma_m^3/G_m^2) \tag{10}$$

where N is Avogadro's number and σ_m is the liquid/crystal interfacial energy per molar surface area. The term σ_m is related to the molar heat of fusion, H_m^f, on the basis of the relationship between bond energy values across the interface [24] and can be expressed as

$$\sigma_m = \alpha H_m^f. \tag{11}$$

Saunders and Miodownik [6] empirically evaluated the constant α to be $\alpha \approx 0.41$.

To apply Eq. (8), it is necessary to derive (or estimate) the quantities η, G^*, and G_m.

The viscosity of the supercooling melts can be described generally using the Vogel–Fulcher–Tammann (VFT) equation, as follows:

$$\eta = \eta_0 \exp\left(\frac{B}{T - T_0}\right) \tag{12}$$

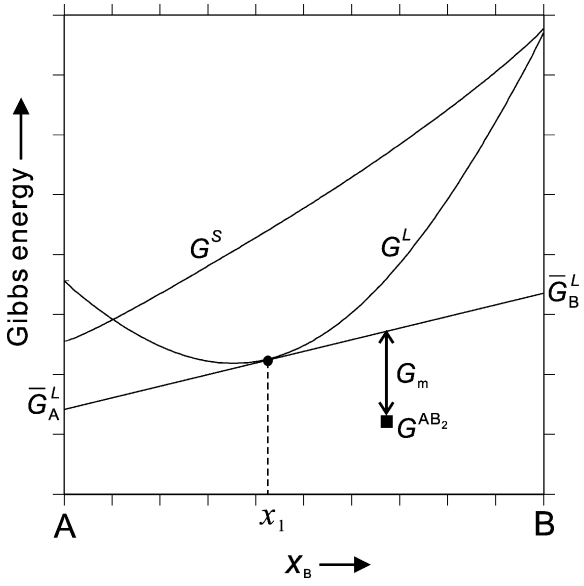

Fig. 1. The construction used in calculating the driving force, G_m, for the crystallization of compound AB_2 from a liquid of composition x_1 in the A–B system.

where η_0, B, and T_0 are empirical parameters. T_0 is the ideal glass transition temperature, and lies near to, but slightly below, the glass transition temperature, T_g. Assuming that $\eta = 10^{12}$ Pa s at T_g together with the experimental data on viscosity of the melts, the parameters in Eq. (12) can be obtained. If T_g data are not available, then the crystallization temperature, T_x, can be used as a first approximation. However, there are few experimental data on the viscosity of the melts. In this case, the viscosity can be approximated as being between the liquidus temperature, T_m, and the glass transition temperature, T_g, using the Doolittle expression based on the relative free volume, f_T, given by the expression [25]

$$\eta = A \exp(B/f_T) \tag{13}$$

where

$$f_T = C \exp(-E_H/RT). \tag{14}$$

The terms A, B, and C are constants, and E_H is the hole formation energy. Because of the lack of experimental data, in this study, E_H was calculated on the basis of the linear relationship between E_H and T_g [25]. Then, assuming that $f_T = 0.03$ and $\eta = 10^{12}$ Pa s at T_g, and assigning a value of $B = 1$, the other constants, A and C, can be evaluated. If T_g data are not available, then the crystallization temperatures, T_x, can be used as a first approximation.

In this study, the viscosities of the Fe–B and Fe–Si–B alloys were evaluated using the Vogel–Fulcher–Tammann equation and the Doolittle expression, respectively.

The molar free energy driving force for liquid to crystal growth, G_m, can be obtained from the thermodynamic phase diagram calculations. It should be noted that, although various models for amorphous phases were proposed as mentioned above, a supercooled liquid phase was described by extrapolation of its high temperature properties in this study. Fig. 1 shows a schematic diagram for calculating the driving force for the crystallization of an AB_2 compound from a supercooled liquid of composition x_1, in a theoretical A–B binary system, where G^L, G^S, and G^{AB_2} denote the Gibbs energy of the liquid, solid solution, and AB_2 phase, respectively. The partial molar Gibbs energies of elements A and B in the liquid phase are denoted by $\overline{G}^L_A$ and $\overline{G}^L_B$, respectively, and represent the chemical potential. In Fig. 1, there is a driving force for the crystallization of the AB_2 compound given by G_m, where G_m represents the Gibbs energy required to form one mole of AB_2 from the liquid of composition x_1. Therefore, G_m is expressed by the following equation:

$$G_m = x_A \overline{G}^L_A + x_B \overline{G}^L_B - G^{AB_2} \tag{15}$$

where x_A and x_B are the mole fractions of elements A and B in the crystalline phase AB_2. For the B2 ordered bcc phase, the driving force was calculated for the composition at which the B2 phase crystallizes primarily from the liquid phase.

In this study, the temperature dependence of G_m was approximated as being linear from the following expression:

$$G_m = H^f_m (T_m - T)/T_m. \tag{16}$$

The value of G^* can be derived by inserting the value of H^f_m into Eq. (11) and using Eq. (10).

The TTT curves were calculated for the Fe–Si–B alloys using the values of η, G^*, and G_m derived using the procedures described above. For the calculation of Eq. (8), the value of $X = 10^{-6}$ was taken following the suggestion of Uhlmann [23], and the values of $a_0 = 0.28 \times 10^{-9}$ m and $N_v = 5 \times 10^{28}$ atoms/m^3 were adopted following Saunders and Miodownik [6] because of the lack of information for quantitative determination of these values. However, the effect of the slight changes in the latter two on the calculated critical cooling rates is less than one order of magnitude.

The critical cooling rates were calculated using the following equation:

$$R_c = \frac{T_m - T_n}{t_n} \tag{17}$$

where T_n and t_n are the temperature and time, respectively, at the nose of the TTT curves.

Table 2
Formation energies of FeB and SiB phases with a B2 structure

Phase	Formation energy (kJ/mol)
FeB	−11.6
SiB	112.6

Each value refers to the bcc Fe, diamond Si, or α-rhombohedral B phases.

Table 3
Evaluated thermodynamic parameters in the Fe–Si–B ternary system

Phase	Symbol	Thermodynamic parameter (J/mol)	Reference
L	${}^{0}L^{\mathrm{L}}_{\mathrm{B,Fe,Si}}$	0	Present work
	${}^{1}L^{\mathrm{L}}_{\mathrm{B,Fe,Si}}$	−50 000	
	${}^{2}L^{\mathrm{L}}_{\mathrm{B,Fe,Si}}$	40 000	
α_2[a]	$G^{\mathrm{ord\_bcc}}_{\mathrm{Fe:B}}(=G^{\mathrm{ord\_bcc}}_{\mathrm{B:Fe}})$	−47 143	
(B2_bcc)	$G^{\mathrm{ord\_bcc}}_{\mathrm{Si:B}}(=G^{\mathrm{ord\_bcc}}_{\mathrm{B:Si}})$	0	
$Fe_{4.7}Si_2B$	$G^{\mathrm{Fe_{4.7}Si_2B}}_{\mathrm{Fe:Si:B}}$	$-231\,865+5T+4.7G^{\mathrm{bcc}}_{\mathrm{Fe}}+2G^{\mathrm{bcc}}_{\mathrm{Si}}+G^{\mathrm{bcc}}_{\mathrm{B}}$	
Fe_5SiB_2	$G^{\mathrm{Fe_5SiB_2}}_{\mathrm{Fe:Si:B}}$	$-234\,579+23T+5G^{\mathrm{diamond}}_{\mathrm{Fe}}+G^{\mathrm{diamond}}_{\mathrm{Si}}+2G^{\mathrm{diamond}}_{\mathrm{B}}$	
$Fe_2Si_{0.4}B_{0.6}$	$G^{\mathrm{Fe_2Si_{0.4}B_{0.6}}}_{\mathrm{Fe:Si:B}}$	$-83\,085.6+7.2T+2G^{\beta\_\mathrm{rhombohedral}}_{\mathrm{Fe}}+0.4G^{\beta\_\mathrm{rhombohedral}}_{\mathrm{Si}}+0.6G^{\beta\_\mathrm{rhombohedral}}_{\mathrm{B}}$	

[a] The ordered α_2 phase has a contribution from the disordered bcc phase.

5. Optimization of the thermodynamic parameters and calculation of the phase diagrams of the Fe–Si–B ternary system

In this study, the thermodynamic parameters of the Fe–Si, Fe–B, and Si–B systems were taken from [17], [26], and [27], respectively.

For the Fe–Si–B ternary system, Aronsson et al. [14] and Efimov et al. [4] have provided the isothermal section diagrams for the Fe-rich corner at 1000 and 900 °C, respectively. The isothermal section at 900 °C over the entire composition range has been reported by Chaban and Kuz'ma [15]. Nagumo and Sato [3] have determined the liquidus temperatures in the Fe-rich corner from the cooling curves of the melts. As already mentioned, three ternary compound phases have been identified in this system: Fe_5Si_2B [4,14,15], $Fe_{4.7}SiB_2$ [4,14,15], and $(Fe, Si)_3B$ [14, 15]. In this study, all these compounds were treated as being stoichiometric, and $(Fe, Si)_3B$ was described using the formula $Fe_2Si_{0.4}B_{0.6}$, based on the experimental composition [14,15].

In the assessment of the thermodynamic parameters of the bcc phase, it is necessary to evaluate the phase stability of the hypothetical FeB and SiB phases with a CsCl-type B2 superstructure, which corresponds to the thermodynamic parameters $G^{\mathrm{ord\_bcc}}_{\mathrm{Fe:B}}(=G^{\mathrm{ord\_bcc}}_{\mathrm{B:Fe}})$ and $G^{\mathrm{ord\_bcc}}_{\mathrm{Si:B}}(=G^{\mathrm{ord\_bcc}}_{\mathrm{B:Si}})$. However, there is no experimental information available to allow us to determine these parameters. Therefore, the enthalpies of formation for FeB and SiB with a B2 structure obtained from ab initio calculations were introduced in the present assessment. The calculations were carried out on the basis of the Full Potential Linearized Augmented Plane Wave (FLAPW) method using the WIEN2k software package [28]. Muffin-tin radii of 2.0 au for Fe and Si, and 1.4 au for B were assumed, and $RK_{\max}$ was fixed at $RK_{\max} = 9.0$, which closely corresponds with the 20 Ryd cut-off energy. The details of the calculation procedure have been described in a previous paper [29]. The results of the ab initio calculations are shown in Table 2, where each value of the formation energy is referred to as either bcc Fe, diamond Si, or α-rhombohedral B. As regards the SiB phase with a B2 structure, no ordering was observed, and hence the parameter $G^{\mathrm{ord\_bcc}}_{\mathrm{Si:B}}(=G^{\mathrm{ord\_bcc}}_{\mathrm{B:Si}})$ was set to zero.

In the present analysis, the thermodynamic parameters were evaluated on the basis of the experimental DSC data and the reported isothermal section diagrams [14,15]. The evaluated parameters in the Fe–Si–B system are listed in Table 3.

The calculated isopleths at the 65 mol% Fe, 10 mol% B, and 10 mol% Si sections are shown in Fig. 2(a)–(c), respectively, together with the DSC data. The expected experimental peaks in the thermal analysis corresponding to the liquidus temperatures were not observed for some of the alloys prepared in Fig. 2(b) and (c). The reason for this is that the thermal arrests were too small for accurately identifying the liquidus temperature. Except for the above result, there was good agreement between the calculated and the experimental DSC results. In Fig. 2(b) and (c), the liquidus temperatures from [3] are also shown, but their values are lower than both the calculated and the experimental DSC results. Taking into account that the amorphization ability of this ternary alloys is relatively high [1–4], the results of Nagumo and Sato seem to have been affected by supercooling, since their values were determined from the cooling curves of the melts.

Fig. 3 shows the calculated isothermal sections at 900 and 1000 °C. The experimental phase equilibria reported by Chaban and Kuz'ma [15] and Aronsson et al. [14], respectively, are shown by the dotted lines in Fig. 3, for comparison with our calculated phase equilibria. From the experimental data, a phase equilibrium between FeB, Fe_5SiB_2, and FeSi was identified at both 900 and 1000 °C. On the other hand, XRD analysis of the prepared alloys

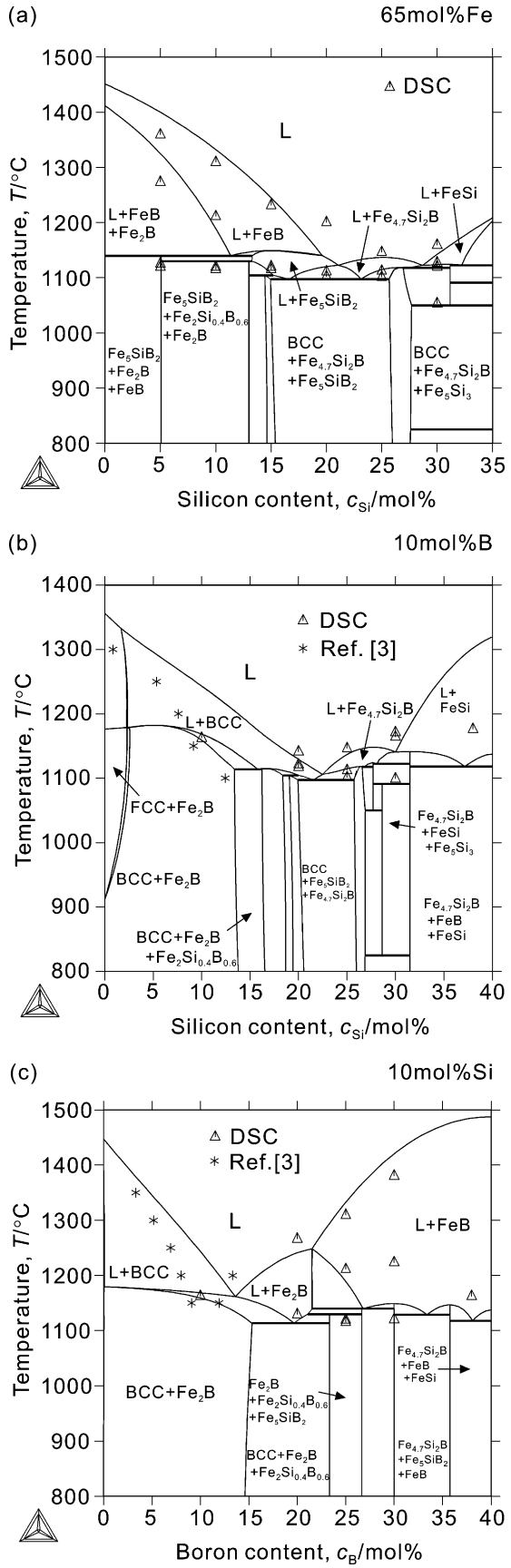

Fig. 2. Calculated isopleths of the Fe–Si–B system at: (a) the 65 mol% Fe, (b) 10 mol% B, and (c) 10 mol% Si sections, and the experimental results.

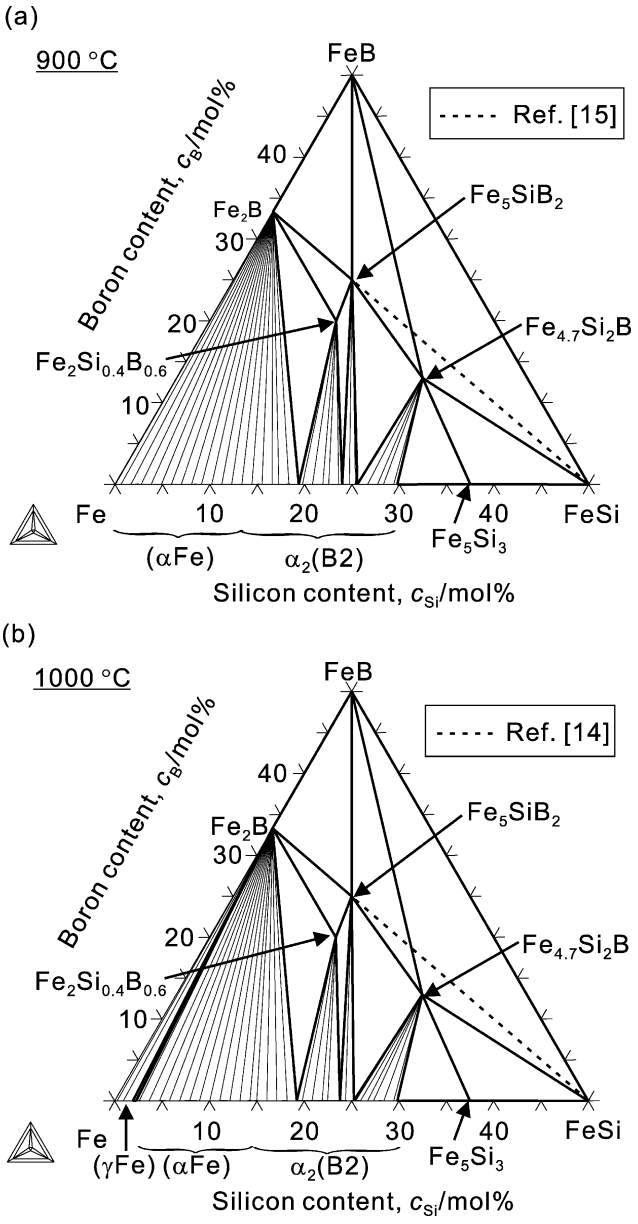

Fig. 3. Calculated isothermal section diagrams of the Fe–Si–B system at: (a) 900 and (b) 1000 °C.

equilibrated at 900 °C showed that a phase equilibrium between FeB, $Fe_{4.7}Si_2B$, and FeSi existed, and this result was adopted in the present analysis. Using these data, the calculated results agree well with the experimental results.

As regards the thermochemical properties in this ternary system, the activity of the components [30] and the enthalpy of mixing in the liquid phase [30,31] have been reported. The calculated activity of Si and the enthalpy of mixing are compared with the experimental ones in Figs. 4 and 5, respectively—the values of activity referred to as liquid components, and the enthalpy of mixing referred to as liquid Fe, Si, and β-rhombohedral B. The changes in both the calculated activity and enthalpy of formation with Si content

Table 4
Alloy compositions used in our calculations, crystallization temperatures, crystalline phases controlling amorphization, and calculated critical cooling rates of the Fe–Si–B ternary alloys

No	Alloy composition (mol%)			T_x (K)	Phase	R_c (K/s)
	Fe	Si	B			
1	89	–	11	640	Fe_3B	1.7×10^6
2	85	–	15	703	Fe_2B	2.8×10^5
3	83	–	17	760 (T_g)	Fe_2B	8.3×10^5
4	80	–	20	728	Fe_2B	8.8×10^5
5	75	–	25	726	Fe_2B	6.8×10^6
6	85	5	10	723[a]	Fe_3B	1.9×10^6
7	85	10	5	653[a]	Fe_3B	1.0×10^6
8	80	15	5	700[a]	$Fe_2Si_{0.4}B_{0.6}$	8.0×10^5
9	80	10	10	818 (T_g)	Fe_2B	1.2×10^4
10	80	5	15	810	Fe_2B	9.6×10^5
11	75	20	5	766[a]	α_2 (B2_bcc)	4.4×10^7
12	75	17.5	7.5	770[a]	α_2 (B2_bcc)	2.5×10^7
13	75	15	10	783[a]	$Fe_2Si_{0.4}B_{0.6}$	4.3×10^5
14	75	10	15	804	Fe_2B	9.8×10^5
15	75	5	20	800[a]	Fe_2B	1.6×10^7
16	72.5	15	12.5	800[a]	α_2 (B2_bcc)	7.0×10^5
17	72.5	10	17.5	800[a]	Fe_2B	3.1×10^6

[a] Values estimated in this study.

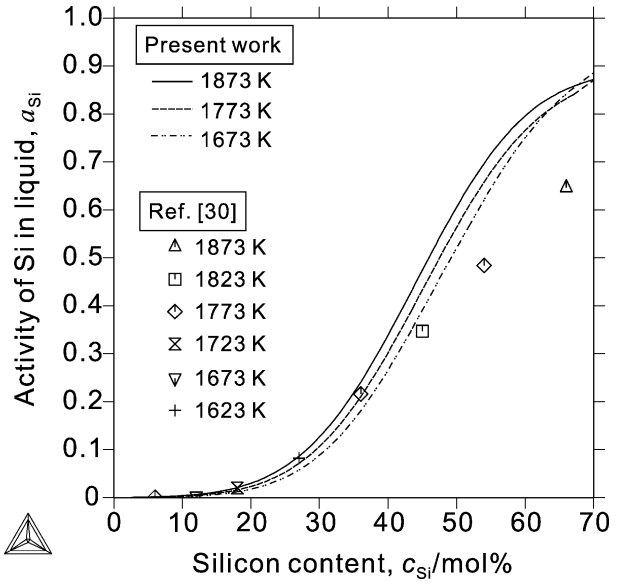

Fig. 4. Variation of the activity of silicon at the section of 25 mol% B in the liquid phase and comparison with the experimental data. Reference states are liquid components.

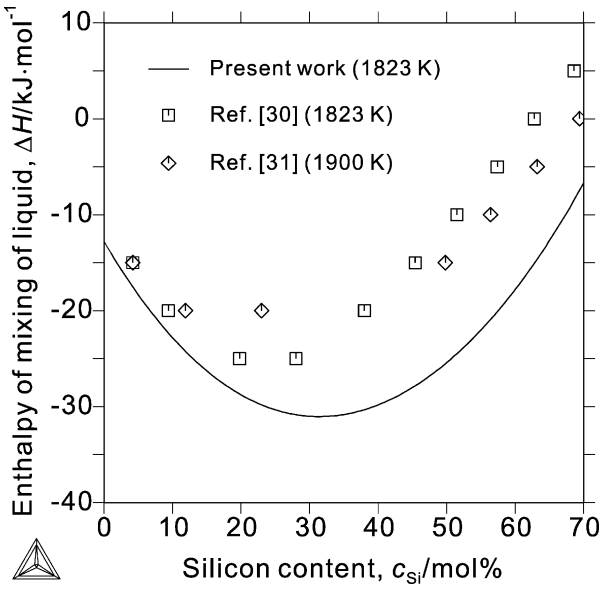

Fig. 5. The enthalpy of mixing of the liquid phase at the section of 25 mol% B at 1823 K compared with the experimental data. Reference states were liquid Fe, Si, and β-rhombohedral B.

agree with the experimental values roughly; however, we could not obtain ternary parameters to fit to the experimental data on thermochemical properties simultaneously with the data on phase boundaries with constituent binary parameters adopted in this study.

6. Evaluation of the glass-forming ability

As regards the experimental glass-forming ability of Fe–Si–B ternary alloys, Inoue et al. [1], Luborsky et al. [2], and Efimov et al. [4] have reported on the compositional amorphization region. Tomut and Chiriac [32] and Yamasaki et al. [33] have reported experimental data on the viscosity of Fe–B binary and Fe–Si–B ternary alloys, respectively. However, data on Fe–Si–B ternary alloys are very limited and, hence, the viscosities of Fe–B binary and Fe–Si–B ternary liquid alloys were evaluated using the Vogel–Fulcher–Tammann equation and the Doolittle expression, respectively. There are no experimental data on the glass transition temperatures, except for

Table 5
Evaluated parameters in the VFT equation of the Fe–B binary alloys

No	Alloy composition (mol%)		η_0 ($\times 10^5$ Pa s)	B (K)	T_0 (K)	Reference
	Fe	B				
1	89	11	8.53	4625	515	[34]
2	85	15	3.50	5696	553	Present work
3	83	17	2.43	4821	634	
4	80	20	1.38	6941	549	
5	75	25	1.56	5181	584	

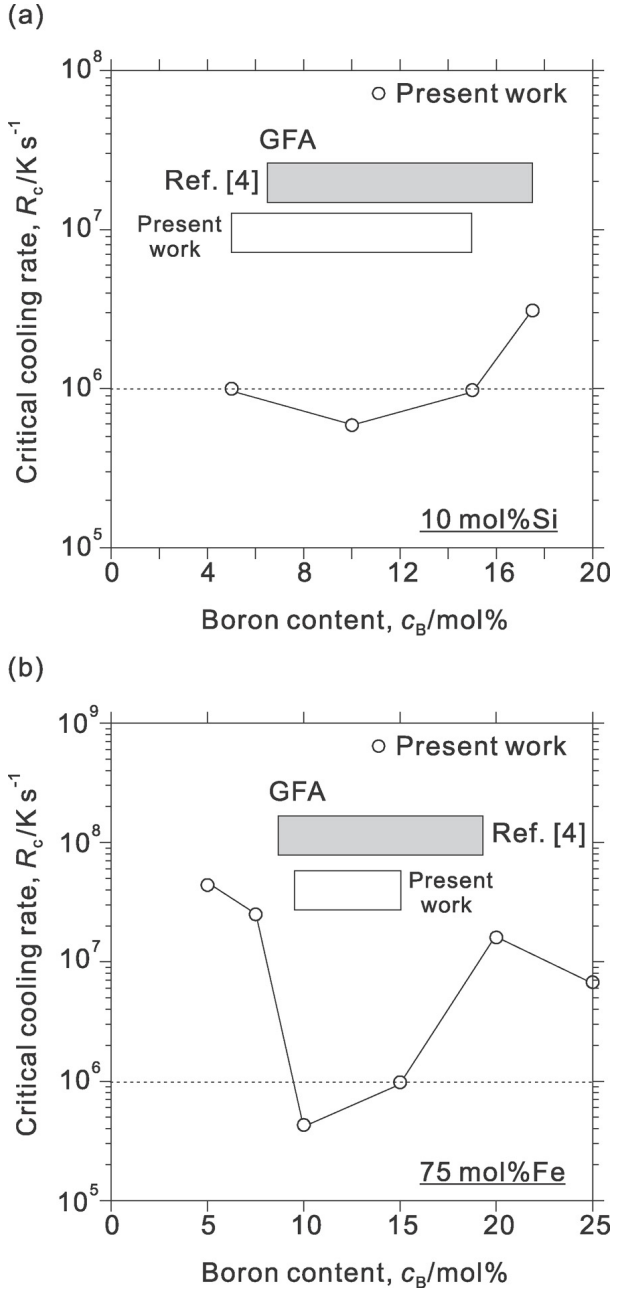

Fig. 6. Calculated critical cooling rates for amorphization at: (a) the 10 mol% Si and (b) 75 mol% Fe sections, with the experimentally observed and calculated glass-forming range at a cooling rate of 10^6 K/s.

Fe–10Si–10B (mol%), which has a glass transition temperature of 818 K [34]. Therefore, the reported crystallization temperatures of the Fe–B binary [35] and Fe–Si–B ternary alloys [1] were used in applying the Doolittle expression. Furthermore, in this study, the crystallization temperatures of some of the ternary alloys were estimated from the experimental result [1], where the change in crystallization temperature with Si and B content was shown with isotherms. The alloy composition concerned, and crystallization temperatures in the present calculations, are listed in Table 4. The parameters used in Eqs. (13) and (14) are shown in Table 5.

The calculated critical cooling rates and crystalline phases that control amorphization are shown in Table 4. Fig. 6 shows the calculated critical cooling rates at the 10 mol% Si and 75 mol% Fe sections. In Fig. 6, the predicted amorphization region at a cooling rate of 10^6 K/s is shown together with the experimental results [4]. In Fig. 7, the calculated critical cooling rates are plotted on the calculated liquidus surface projection, where open circles and circles with crosses denote critical cooling rates $<10^6$ K/s and critical cooling rates $>10^6$ K/s, respectively. The experimental compositional regions of amorphization reported by Inoue et al. [1] and Efimov et al. [4] (dotted and broken lines, respectively) are also shown in Fig. 7. There was good agreement between the calculated glass-forming ability and the experimental glass-forming abilities.

7. Conclusions

A thermodynamic analysis of the Fe–Si–B ternary system was carried out by combining experimental results from differential scanning calorimetry with literature data. The glass-forming ability of this alloy system was evaluated by introducing the thermodynamic quantities obtained from the phase diagram calculations into the Davies–Uhlmann kinetic formulations. The results obtained can be summarized as follows:

(1) The calculated phase boundaries of the Fe–Si–B system agree well with our experimental DSC results. The phase equilibria between FeB, $Fe_{4.7}Si_2B$, and FeSi were determined at 900 °C using XRD analysis, compared with the phase equilibria between FeB, Fe_5SiB_2, and FeSi reported by Chaban and Kuz'ma.

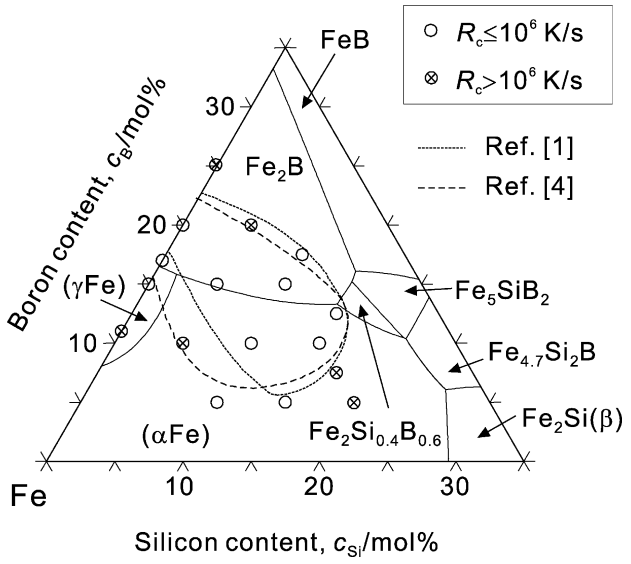

Fig. 7. Comparison of the calculated and experimental glass-forming abilities of Fe–Si–B ternary alloys on the calculated liquidus surface projection.

(2) The calculated glass-forming ability of Fe–Si–B ternary alloys was in good agreement with the experimental compositional amorphization range.

Acknowledgements

We acknowledge use of the Thermo-Calc software program in the phase diagram calculations. One of authors (T.T.) acknowledges financial support from the Naito Taisyun Science and Technology Foundation.

References

[1] A. Inoue, T. Masumoto, M. Kikuchi, T. Minemura, J. Japan Inst. Metals 42 (1978) 294–303.
[2] F.E. Luborsky, J.J. Becker, J.L. Walter, H.H. Liebermann, IEEE Trans. Magn. MAG-15 (1979) 1146–1149.
[3] M. Nagumo, T. Sato, Suppl. Sci. Rep. RITU., A (1980) 136–142.
[4] Yu.V. Efimov, G.G. Mukhin, E.M. Lazarev, N.A. Korotkov, L.A. Ryabtsev, V.N. Dmitriev, T.M. Frolova, Russ. Metall. 4 (1986) 167–173.
[5] H.A. Davies, Phys. Chem. Glasses 17 (1976) 159–173.
[6] N. Saunders, A.P. Miodownik, Mater. Sci. Technol. 4 (1988) 768–777.
[7] N. Saunders, Int. J. Rapid Solidif. 1 (1984) 327–330.
[8] S.H. Zhou, J. Schmid, F. Sommer, Thermochimica Acta 339 (1999) 1–9.
[9] O. Tolochko, J. Ågren, J. Phase Equilib. 21 (2000) 19–24.
[10] G. Shao, J. Appl. Phys. 88 (2000) 4443–4445.
[11] Y.Q. Liu, G. Shao, K.P. Homewood, J. Appl. Phys. 90 (2001) 724–727.
[12] M. Palumbo, G. Cacciamani, E. Bosco, M. Baricco, CALPHAD 25 (2001) 625–637.
[13] N. Saunders, A.P. Miodownik, CALPHAD, A Comprehensive Guide, Pergamon, Elsevier Science Ltd, Oxford, 1998.
[14] B. Aronsson, I. Engström, Acta Chem. Scand. 14 (1960) 1403–1413.
[15] N.F. Chaban, Yu.B. Kuz'ma, Inorg. Mater. 6 (1970) 883–884.
[16] A.T. Dinsdale, CALPHAD 15 (1991) 317–425.
[17] J. Lacaze, B. Sundman, Metall. Trans. A 22A (1991) 2211–2223.
[18] M. Hillert, L.-I. Staffansson, Acta Chem. Scand. 24 (1970) 3618–3626.
[19] I. Ansara, N. Dupin, H.L. Lukas, B. Sundman, J. Alloys Compounds 247 (1997) 20–30.
[20] J.F. Löffler, J. Schroers, W. Johnson, Appl. Phys. Lett. 77 (2000) 681–683.
[21] K.F. Kelton, A.L. Greer, J. Non-Cryst. Solids 79 (1986) 295–309.
[22] G. Shao, P. Tsakiropoulos, Acta Metall. Mater. 42 (1994) 2937–2942.
[23] D.R. Uhlmann, J. Non-Cryst. Solids 7 (1972) 337–348.
[24] D. Turnbull, J. Appl. Phys. 21 (1950) 1022–1028.
[25] P. Ramachandrarao, B. Cantor, R.W. Cahn, J. Mater. Sci. 12 (1977) 2488–2502.
[26] L.-M. Pan, in: B. Sundman (Ed.), Division of Computational Thermodynamics, SGTE Solution Database, ver. 2, Royal Institute of Technology, Stockholm, Sweden, 1994.
[27] T. Tokunaga, K. Nishio, H. Ohtani, M. Hasebe, Mater. Trans. 44 (2003) 1651–1654.
[28] P. Blaha, K. Schwarz, G. Madsen, D. Kvasnicka, J. Luitz, WIEN2k, 2004. http://www.wien2k.at/.
[29] T. Tokunaga, K. Hashima, H. Ohtani, M. Hasebe, Mater. Trans. 45 (2004) 1507–1514.
[30] A.I. Zaitsev, N.E. Zaitseva, A.A. Kodentsov, Metall. Mater. Trans. B 34B (2003) 887–898.
[31] V.T. Witusievicz, A.A. Shcheretskii, A.K. Biletskii, V.S. Schumikhin, Rasplavy 4 (1989) 102–103.
[32] M. Tomut, H. Chiriac, Mater. Sci. Eng. A 304–306 (2001) 272–276.
[33] T. Yamasaki, T. Shimada, Y. Ogino, J. Japan Inst. Met. 56 (1992) 1229–1234.
[34] H.A. Davies, Proceedings of the Third International Conference on Rapidly Quenched Metals, The Metal Society, London, 1978, pp. 1–21.
[35] T. Nakajima, I. Nagami, H. Ino, J. Mater. Sci. Lett. 5 (1986) 60–62.